Antonina MAIZELIS, Boris BAIRACHNYI

CORROSION PROPERTIES OF $(Zn\text{-}Ni)_1/(Zn\text{-}Ni)_2$ MULTILAYER COATINGS

National Technical University "Kharkiv Polytechnic Institute"
2, Kyrpychova St, Kharkiv, 61002, Ukraine. E-mail: a.maizelis@gmail.com

ABSTRACT

A study of corrosion behavior of multilayer coatings $(Zn\text{-}Ni)_1/(Zn\text{-}Ni)_2$ in comparison with single-layer coatings of Zn-Ni alloy of similar chemical composition is presented. The coatings were deposited from pyrophosphate-citrate electrolyte. Multilayer coatings were obtained by a two-pulse galvanostatic method. It is shown that increase in nickel content in the coating leads to the shift of the corrosion potential of multilayer coatings in 3.5 % NaCl toward more positive value. When average nickel content is 23-24 wt.%, the corrosion potentials is close to the value for cadmium coatings. Long-term exposure of steel samples with coatings of 10 μm thickness in a renewable 3,5 % NaCl solution showed that as compared with single-layer coatings, zinc dissolute from the multilayer coatings until the coating reaches the potential of the steel surface at 2.6 times slower in the case of coatings consisting mainly γ-phase, 2.2 times slower in the case of Zn-enriched coatings, and 1.5 times slower in the case of nickel-enriched coatings enriched.

***KEY WORDS**: multilayer coating, corrosion, Zn-Ni, alloy.*

INTRODUCTION

Zinc plating is widely used in protecting steel surfaces from corrosion. Having a much more negative potential, zinc in contact with carbon steels dissolves under the influence of the environment, protecting steel from corrosion damage. In turn, zinc surface needs protection from rapid dissolution, therefore it is passivated. A more reliable way to increase the life of zinc coatings is to alloy it with metals of the iron group. The most successfully used coating is Zn-Ni alloy. Increase in nickel content in the alloy leads to decrease in the corrosion rate of the coating. However, potential of the coating increases reducing protective ability of the coating. Therefore, nickel content in the alloy is limited by the composition providing the cathodic nature of the protection of steel.

Numerous studies have shown that the corrosion currents of nanocrystalline coatings are significantly lower than alloy coatings with coarser crystals [1]. Corrosion currents also decrease in the case of nanocomposite coatings [2] and coating deposited under pulsed current [3, 4]. The rate of corrosion of multilayer coatings consisting of alternating layers of zinc and nickel [5], Zn-Ni alloy and nickel [6] or Ni-P alloy [7] of 0.5-3 μm thickness deposited using duel-baths technique is low. Recently, the processes of obtaining multilayer coatings consisting of alternating layers of Zn-Ni alloys that are even thinner (50-500 nm) deposited by single-bath technique from various acidic electrolytes [8-11] including compositional additives [12, 13] are actively studied. Corrosion resistance of coatings significantly depends on the properties of the electrolyte and the electrolysis mode. On the one hand, it is shown that in the case of single-layer coatings of Zn-Ni alloy, corrosion resistance of coatings prepared from complex alkaline electrolytes [14-16] is higher. On the other hand, multilayer coatings based on other alloys, obtained from polyligand electrolytes, have improved mechanical and anticorrosion properties [17-19]. Therefore, it is of interest to obtain $(Zn\text{-}Ni)_1/(Zn\text{-}Ni)_2$ multilayer coatings from a polyligand pyrophosphate-citrate electrolyte.

The aim of the study is to compare the corrosion behavior of multilayer coatings with single-layer coatings of the same chemical composition obtained from pyrophosphate-citrate electrolyte and containing mainly γ-phase, as well as zinc- and nickel-enriched films.

MATERIALS AND METHODS

Zn-Ni alloy coatings and $(Zn\text{-}Ni)_1/(Zn\text{-}Ni)_2$ multilayer coatings were deposited on Steel 3 substrate (4.5 cm^2) from pyrophosphate-citrate electrolytes (*E1* and *E2*, Table 1). Electrochemical studies were performed using P-45X potentiostat with three-electrode cell including (1) working electrodes were made steel, platinum, and steel with Zn-Ni alloy coatings, (2) counter electrode made

of platinum or combined zinc-nickel, and (3) saturated silver chloride reference electrode. All the potentials are presented *vs.* this electrode.

Table 1. Electrolyte composition

Electrolyte component	Electrolyte	
	E1	*E2*
$NiSO_4$, mol L^{-1}	0.1	0.15
$ZnSO_4$, mol L^{-1}	0.2	0.15
$K_4P_2O_7$, mol L^{-1}	0.6	
K_3Cit, mol L^{-1}	0.15	
KCl, g L^{-1}	15	
pH	8.5	

Anodic voltammograms of alloy films were obtained in an alkaline (pH 10.5) ammonia-glycinate electrolyte *E3* containing 0.5 mol l^{-1} glycine and 0.5 mol l^{-1} NH_4Cl. Alloy single-layer coatings were deposited by galvanostatic and multilayer coatings were deposited by two-pulse galvanostatic methods with stirring by magnetic stirrer. The corrosion behavior was studied in aerated 3.5 % NaCl solution. The composition of the alloy coatings was determined by X-ray fluorescence (XRF) method.

RESULTS AND DISCUSSION

Cyclic voltammograms in pyrophosphate-citrate electrolytes for Zn-Ni alloy coatings electrodeposition are presented in Fig. 1. The cathode branches of cyclic voltammograms begin from the region of nickel deposition potentials, and the first part of cyclic voltammogram in *E2* electrolyte (curve 2) is higher than in *E1* electrolyte, due to the higher nickel ions content in it. Sharp increase in current is observed on the cathode branch of cyclic voltammograms due to hydrogen evolution at potentials below –1.4 V.

The backward branches of cyclic voltammograms above the limiting current practically repeat their forward parts indicating a very slight development of the surface at high current density. Before the limiting current, the backward branches are significantly below the forward brunches, illustrating the significant inhibition of nickel discharge during alloy deposition. The anode branches of cyclic voltammograms in both electrolytes have the same set of peaks, however in *E1* electrolyte (curve 1) the peak height of zinc dissolution at the most negative potentials is higher than in *E2* electrolyte (curve 2). On the contrary, the area of the peaks of dissolution of nickel-enriched phases at higher potentials is larger in the *E2* electrolyte in comparison with *E1* electrolyte.

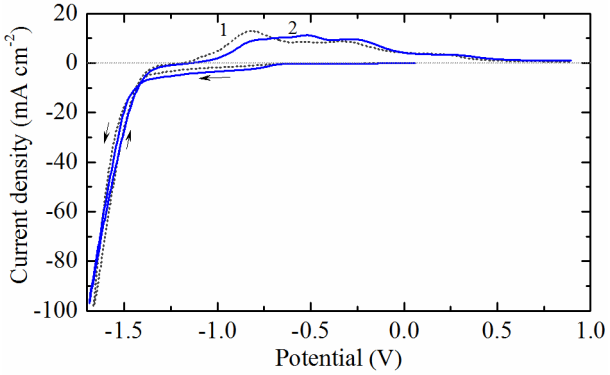

Fig. 1. Cyclic voltammograms on Pt in *E1* (1) and *E2* (2) electrolytes. Potential scan rate is 50 mV s^{-1}.

Chronopotentiograms of deposition of thin alloy films constituting multilayer coatings are shown in Fig. 2. All of them start from the region of nickel deposition potentials and reach alloy deposition potentials. In the case of 40 and 60 mA cm^{-2} this process occurs very quickly.

In the *E2* electrolyte with a higher content of nickel ions, the anodic voltammogram of the film dissolution obtained at 2 mA cm^{-2} (Fig. 3 *a*, curve 2) has only one dissolution peak of nickel-enriched phase (>50 % Ni) with subsequent plateau of nickel passivation. In the *E1* electrolyte, a film

deposited at the same current density has γ-phase in its composition, since a peak of zinc dissolution from γ-phase appears to the left of the peak of nickel-enriched phase dissolution (curve 1).

At a current density of 40 mA cm^{-2}, a peak of zinc dissolution from γ-phase is also detected on the anode polarization curve of the film obtained in *E2* electrolyte (Fig. 3 *b*, curve 2). At anodic voltammogram obtained on a film of electrolyte *E1*, obtained at lower potentials, a doublet peak of dissolution of the zinc phase (or η-phase, containing up to 1% nickel) appears (curve 1).

Anode polarization curves obtained on films deposited at 60 mA cm^{-2} (Fig. 3 *c*) do not qualitatively differ from curves of films obtained at 40 mA cm^{-2}. It indicates the constancy of the alloy composition in this range of current densities.

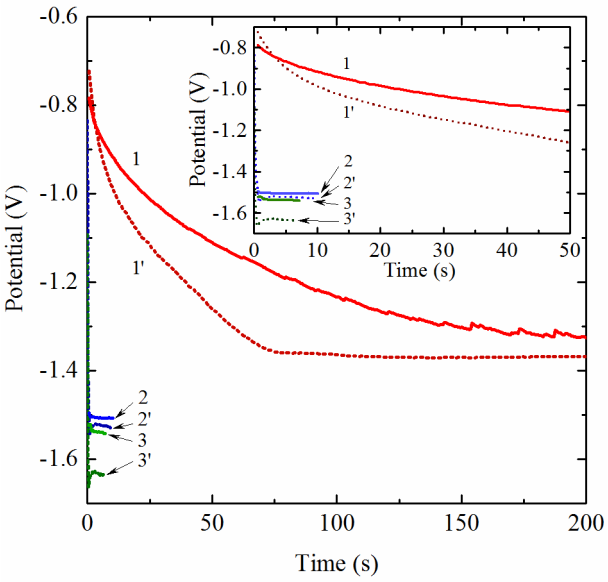

Fig. 2. Potential-time plots of deposition of the Zn-Ni alloy films in *E2* (1, 2, 3) and *E1* (1', 2', 3') electrolytes. Current density of electrodeposition: 2 mA cm^{-2} (1,1'); 40 mAcm^{-2} (2,2'); 60 mA cm^{-2} (3,3').

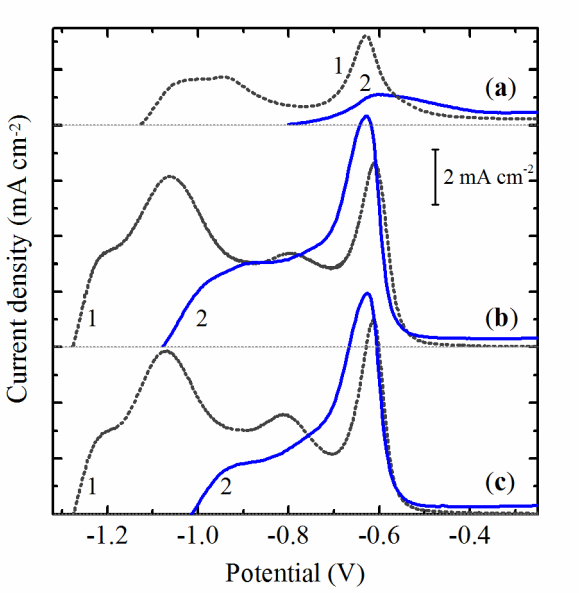

Fig. 3. Anodic polarization curves in ammonia-glycinate electrolyte *E3* on the films obtained in *E1* (1) and *E2* (2) electrolytes. Current density of electrodeposition: (*a*) 2 mA/cm^2; (*b*) 40 mA/cm^2; (*c*) 60 mA/cm^2.

Coatings with a thickness of 10 μm containing zinc excess as compared with γ-phase were deposited from electrolyte *E1*. A single-layer coating (*SL1*) was obtained at a current density of 40 mA cm^{-2}. Multilayer coating (*ML1*) was formed in a two-pulse galvanostatic mode: (1) 14 s at a current density of 30 mA cm^{-2}, (2) 6 s at a current density 80 mA cm^{-3}. The calculated sublayer thickness is 91.0-91.8 nm. Chronopotentiograms of coatings deposition are shown in Fig. 4. Both coatings contained 11.2 % nickel according to the results of XRF analysis. The values of the deposition potentials of a single-layer coating (curve 2) are close to the values of the potential of sublayers of multilayer coating deposition at 30 mA cm^{-2}.

Chronopotentiograms of coatings deposition from an electrolyte with a higher concentration of nickel ions are shown in Fig. 5. The coating contains mainly γ-phase of the alloy. The *ML2* coating was deposited in a two-pulse galvanostatic mode: (1) 60 s at a current density of 6,5 mA cm^{-2}, (2) 40 s at a current density 15 mA cm^{-3}. The estimated thickness of the sublayers of the multilayer coating is 52.7-53.7 nm. The potential of deposition of single-layer coating at current density of 10 mA cm^{-2} (curve 2) is between the deposition potentials of the sublayers of multilayer coating (curve 1) in first 30 min. Then the potential of *SL2* coating deposition is practically equal to the value of base layers of multilayer coating.

Unlike previous coatings (Fig. 4 and Fig. 5, curve 2), the chronopotentiogram of galvanostatic *SL3* coating deposition at 6.5 mA cm^{-2} (Fig. 6, curve 1), which has an excess of nickel in comparison with γ-phase, is more stable. The *ML3* coating was deposited in a two-pulse galvanostatic mode: (1) 40 s at a current density of 10 mA cm^{-2}, (2) 10 s at a current density 40 mA cm^{-3}.

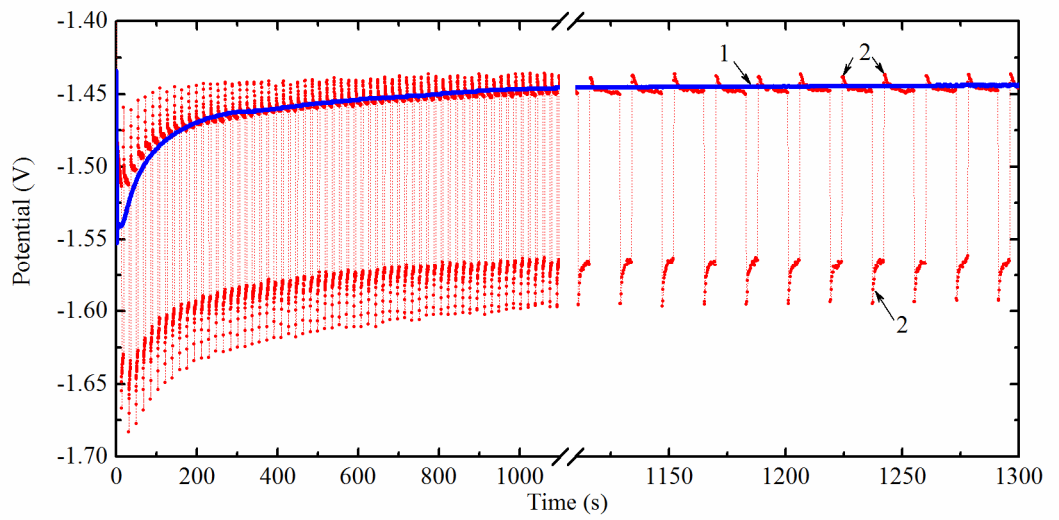

Fig. 4. Potential-time plots of deposition of the coatings containing 11,2 % Ni from E1 electrolyte: (1) multilayer coating (*ML1*), (2) single-layer of alloy (*SL1*).

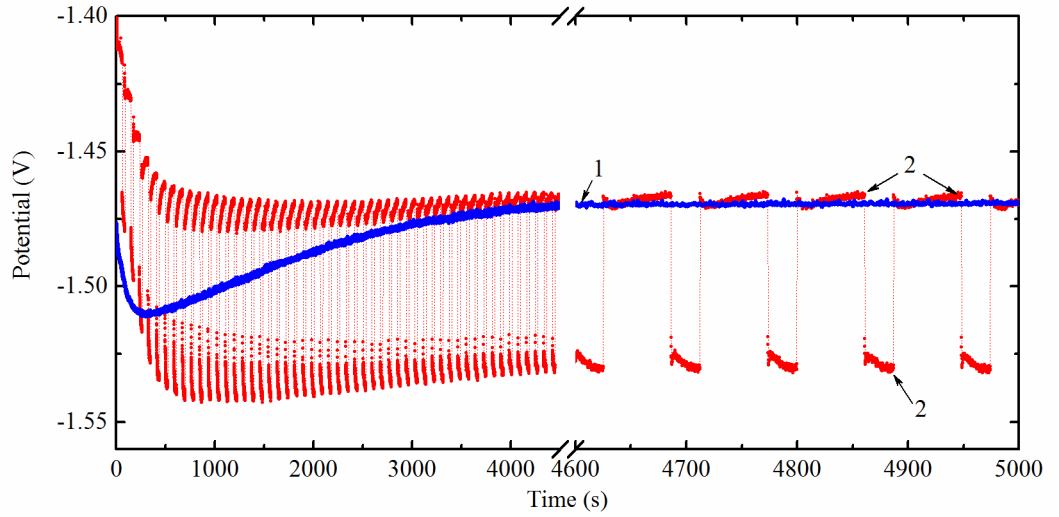

Fig. 5. Potential-time plots of coatings deposition from E2 electrolyte: (1) multilayer coating (ML2) with 16,47 % Ni, (2) single-layer alloy coating (SL2) with 15,34 % Ni.

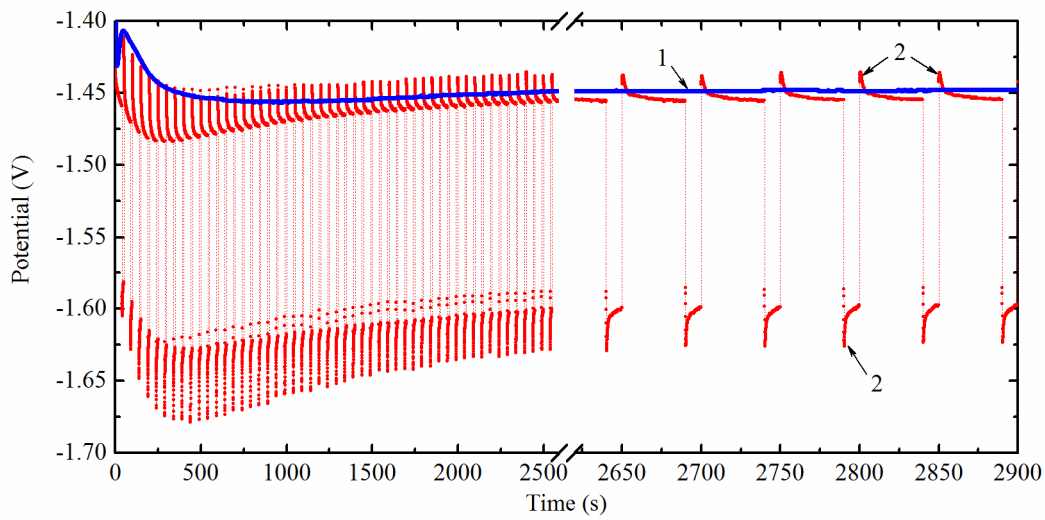

Fig. 6. Chronopotentiograms of *ML3* coating deposition (1) with nickel content of 23,2 %, and *SL3* coating (2) containing 24,0 % Ni.

The estimated thickness of the sublayers of the multilayer coating is 52.5-53.1 nm. The value of the potential of *SL3* coating deposition is close to the potential of deposition of the base sublayers of the *ML3* multilayer coating (curve 2).

The initial corrosion potentials of multilayer coatings in 3.5 % NaCl solution shift upward with an increase in nickel content in the coating (Fig. 7).

The potentials remain more negative (–0.72 V) than the potential of mild steel (–0.6 V) in this solution even in the case of excess of nickel as compared to γ-phase composition. Corrosion potential of these coatings are close to the value of cadmium coating.

During prolonged exposure in NaCl solution with periodic renewal of the solution, which was saturated with corrosion products the corrosion potentials of all samples are shifted upwards due to zinc dissolution from the coating. Then the steel potential values are reached and corrosion of steel begins in the pores and the values of potential decrease.

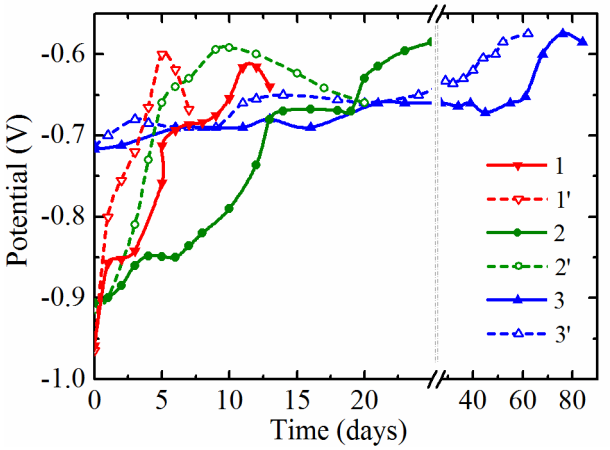

Fig. 7. Change in corrosion potential of *ML1* (1), *SL1* (1'), *ML2*(2), *SL2* (2'), *ML3* (3), *SL3* (3') coatings in 3,5 % NaCl solution.

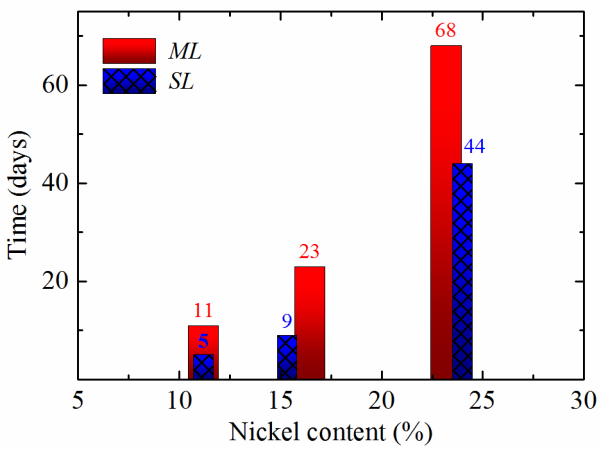

Fig. 8. Time to reach the corrosion potential of steel substrate by the samples with multilayer coatings (*ML*) compared to single-layer coatings (*SL*) by the alloy of the comparable composition.

The rate of change of potential is the highest for zinc-enriched coatings (*ML1* and *SL1*, curve 1 and curve 1'), and the slowest for coatings having an excess nickel content as compared to *γ*-phase (*ML3* and *SL3*, curve 3 and 3'). Compared to single-layer coatings, the rate of change of the corrosion potentials of multilayer coatings is slower (compare curves 1 and 1', 2 and 2', 3 and 3').

The delays in potential change at –0.85 V and in the range of –0.65... –0.7 V for samples with multilayer coatings, are more significant. These potentials correspond to the dissolution of free zinc and zinc (or *η*-phase) from *γ*-phases, respectively [20].

The time to reach the corrosion potential of a steel sample is shown in Fig. 8. In fact, the loss of the ability of single-layer coatings to electrochemically protect the steel substrate occurs faster than in the case of multilayer coatings. The advantage of multilayer coatings is especially evident when nickel content is close to *γ*-phase composition, as the time to reach the steel potential increases by 2.6 times. This period increases by 1.5 times for the samples with nickel excess (column 3) and 2.2 times for samples with zinc excess (column 1).

CONCLUSIONS

The corrosion behavior of single-layer coatings of Zn-Ni alloy deposited under galvanostatic conditions and multilayer coatings $(Zn\text{-}Ni)_1/(Zn\text{-}Ni)_2$ obtained by the two-pulse galvanostatic method having a similar chemical composition are compared.

The alloys were deposited from pyrophosphate-citrate electrolyte. It is shown that with an increase in the nickel content in the coating, the corrosion potential in 3.5 % NaCl solution of steel samples with alloy coatings shifts to more positive values and the time to reach potential of the steel substrate increases during long-term exposure of the samples in solution.

Compared to single-layer coatings, zinc dissolution from multilayer coatings having similar average chemical composition occurs 2.6 times slower for coatings consisting mainly of the γ-phase, 2.2 times slower for Zn-enriched coatings, and 1.5 times slower in the case of Ni-enriched coatings.

REFERENCES

1. Mosavat S. H., Shariat M. H., Bahrololoom M. E. Study of corrosion performance of electrodeposited nanocrystalline Zn–Ni alloy coatings // Corrosion Science. – 2012. – Vol. 59. – P. 81–87.
2. Praveen B. M., Venkatesha T. V. Electrodeposition and properties of Zn–Ni–CNT composite coatings / Journal of alloys and compounds. – 2009. – Vol. 482. – № 1–2. – P. 53–57.
3. Corrosion behavior of reverse-pulse electrodeposited Zn-Ni alloys in saline environment / Y. Boonyongmaneerat, K. Saengkiettiyut, S. Saenapitak, S. Sangsuk // Journal of materials engineering and performance. – 2014. – Vol. 23. – № 1. – P. 302–307.
4. Electrodeposition of zinc–nickel alloy by pulse plating using non-cyanide bath / S. Mohan, V. Ravindran, B. Subramanian, G. Saravanan // Transactions of the IMF. – 2009. – Vol. 87. – № 2. – P. 85–89.
5. Rahsepar M., Bahrololoom M. E. Corrosion study of Ni/Zn compositionally modulated multilayer coatings using electrochemical impedance spectroscopy // Corrosion science. – 2009. – Vol. 51. – № 11. – P. 2537–2543.
6. Corrosion resistance of Zn–Ni/Ni and Ni/Zn–Ni compositionally modulated multilayer coating / J.L. Chen, J.H. Liu, S.M. Li, M. Yu // Materials and Corrosion. – 2012. – Vol. 63, № 7. – P. 607–613.
7. Fabrication of Zn-Ni/Ni-P compositionally modulated multilayer coatings // J.H. Liu, J.L. Chen, Z. Liu, M. Yu, S.M. Li // Materials and Corrosion. – 2013. – Vol. 64. – № 4. – P. 335–340.
8. Bahadormanesh B., Ghorbani M. Ni-P/Zn-Ni compositionally modulated multilayer coatings–Part 2: Corrosion and protection mechanisms // Applied Surface Science. – 2018. – Vol. 442. – P. 313–321.
9. Rashmi S., Elias L., Hegde A. C. Multilayered Zn-Ni alloy coatings for better corrosion protection of mild steel // Engineering science and technology, an international journal. – 2017. – Vol. 20. – № 3. – P. 1227–1232.
10. Bahadormanesh B., Ghorbani M., Kordkolaei N. L. Electrodeposition of nanocrystalline Zn/Ni multilayer coatings from single bath: Influences of deposition current densities and number of layers on characteristics of deposits // Applied Surface Science. – 2017. – Vol. 404. – P. 101–109.
11. Bahadormanesh B., Ghorbani M. Electrodeposition of Zn–Ni–P compositionally modulated multilayer coatings: An attempt to deposit Ni–P and Zn–Ni alloys from a single bath // Electrochemistry Communications. – 2017. – Vol. 81. – P. 93-96.
12. Ullal Y., Chitharanjan Hegde A. Multilayer Zn-Ni-Al2O3 coatings for corrosion protection // International Journal of Materials Engineering Innovation. – 2014. – Vol. 5. – № 3. – P. 247–260.
13. Ullal Y., Hegde A. C. Corrosion protection of electrodeposited multilayer nanocomposite Zn-Ni-SiO_2 coatings // Surface Engineering and Applied Electrochemistry. – 2013. – Vol. 49. – № 2. – P. 161–167.
14. Conde A., Arenas M. A., De Damborenea J. J. Electrodeposition of Zn–Ni coatings as Cd replacement for corrosion protection of high strength steel // Corrosion Science. – 2011. – Vol. 53. – № 4. – P. 1489–1497.
15. Corrosion mechanism of nanocrystalline Zn–Ni alloys obtained from a new DMH-based bath as a replacement for Zn and Cd coatings / Z. Feng, M. An, L. Ren, J. Zhang, P. Yang, Z. Chen // RSC advances. – 2016. – Vol. 6. – № 69. – P. 64726–64740.
16. Electrochemical behaviors and properties of Zn-Ni alloys obtained from alkaline Non-cyanide bath using 5, 5′-dimethylhydantoin as complexing agent / Z. Feng, Q. Li, J. Zhang, P. Yang, M. An // Journal of the Electrochemical Society. – 2015. – Vol. 162. – № 9. – P. D412–D422.
17. Maizelis A.A., Bairachniy B.I., Trubnikova L.V., Savitsky B.A. The effect of architecture of the Cu/(Ni-Cu) multilayer coatings on their microhardness // Functional Materials. – 2012. – Vol. 19, № 2. – P. 238–244.
18. Maizelis A.A., Bairachniy B.I. Electrochemical Formation of Multilayer Metal and Metal-Oxide Coatings in Complex Electrolytes // Springer Proceedings in Physics. – Switzerland, 2017. – Chapter 41. – P. 557–572.
19. Maizelis A. Multilayer Nickel–Copper Anode for Direct Glucose Fuel Cell // Journal of Electrochemical Energy Conversion and Storage. – 2019. – Vol. 16, № 4. – P. 041003.
20. Danilov F. I., Shevlyakov I. A., Mandryka M. M. Phase compositions and corrosion properties of Zn-Ni coatings deposited from alkaline electrolytes // Russian journal of electrochemistry. – 1999. – Vol. 35, № 12. – P. 1322–1326.